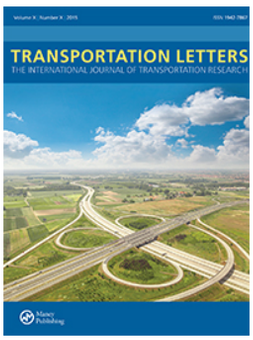

Taylor & Francis
Taylor & Francis Group

Transportation Letters

The International Journal of Transportation Research

ISSN: 1942-7867 (Print) 1942-7875 (Online) Journal homepage: https://www.tandfonline.com/loi/ytrl20

Evaluating the effect of MIPM on vehicle detection performance

Nastaran Yaghoobi Ershadi, José Manuel Menéndez & David Jiménez Bermejo

To cite this article: Nastaran Yaghoobi Ershadi, José Manuel Menéndez & David Jiménez Bermejo (2019): Evaluating the effect of MIPM on vehicle detection performance, Transportation Letters, DOI: 10.1080/19427867.2019.1585682

To link to this article: https://doi.org/10.1080/19427867.2019.1585682

Published online: 08 Mar 2019.

TRANSPORTATION LETTERS
https://doi.org/10.1080/19427867.2019.1585682

Taylor & Francis
Taylor & Francis Group

Evaluating the effect of MIPM on vehicle detection performance

Nastaran Yaghoobi Ershadi, José Manuel Menéndez and David Jiménez Bermejo

E.T.S. Ingenieros de Telecomunicación, Universidad Politécnica de Madrid, Madrid, Spain

ABSTRACT

The introduction of new techniques to improve the robustness and accuracy of vehicle detection is always important for the intelligent transportation system as it may face different problems and challenges. Conventional image-based vehicle detection methods have presented difficulties in acquiring good images due to perspective and background noise, poor lighting and weather conditions. We propose a high-accurate, vehicle detection method by using Modified Inverse Perspective Mapping. Thus, the perspective effect is removed, and then the Hough transform was applied to extract road lines and lanes. Gaussian Mixture Model and chromaticity-based strategy were applied to segment the moving vehicles and tackle shadow effects, respectively. We evaluated the performance of the proposed method under recorded videos in Madrid and Tehran (with different weather conditions at urban and interurban areas). Results indicate that the proposed approach is feasible, and more accurate compared to others, especially when facing bad weather conditions and lighting variations in different environments.

KEYWORDS

Inverse Perspective Mapping; Image transformation; MIPM; GMM; Vehicle detection; Detection accuracy; Counting; Bad weather conditions

Introduction

Today, many researchers are attracted to traffic because it has become a significant problem in our life. With continuous urban road development and construction of highways, the accuracy of vehicle detection became more considerable between researchers. As the main task in ITS, vehicle detection aims to provide valuable information for multiple applications such as vehicle counting, vehicle speed measurement, automatic incident detection, and traffic flow prediction. Various approaches have been proposed and applied to gather such traffic-related information. A diversity of sensing manners have become available for vehicle detection. Video camera (Chen et al. 2014; Liang et al. 2015; Zhang et al. 2013), laser sensors (Mecocci and Micheli 2008), Wireless sensor network (Zhu et al. 2014), LIDAR (Cheng et al. 2014), inductive loop (Sheik Mohammed Ali et al. 2011), microwave radar (Horne et al. 2016; Hilleary and Omar 2012), magnetic sensors (Bugdol, Segiet, and Krecichwost 2014; Markevicius et al. 2016; Dong et al. 2018), ultrasonic sensors (Agarwal, Murali, and Chandramouli 2009; Kim and Eun 1998) and acoustics (Cevher, Chellappa, and McClellan 2009) that are in the market. Traditional methods used hardware (Celik and Kusetogullari 2010) such as inductive loop, radar, and laser to detect vehicles, but the disadvantages are high maintenance cost and being affected by environmental factors (Wang et al. 2017). In contrast, video cameras are more useful in terms of cost and flexibility.

Vision-based techniques are one of the most common approaches to analyze vehicles from images or videos (Veena Ramakrishnan, Prabhavathy, and Devishree 2012). A monocular camera helps to maintain low-cost hardware and high-performance system (Velazquez-Pupo et al. 2018). Moreover, advances in analytical techniques for processing video data, and increased computing power may now provide added value to cameras by automatically extracting related traffic information.

The inverse perspective mapping (IPM) is used to obtain a bird's eye view of the scene from a perspective image. Also, it can be used to remove perspective distortion. In general, each proposed inverse perspective mapping method uses different transformation mechanisms. The performance of methods based on IPM is exacerbated by the perspective and the geometric properties of the objects in an image which has been distorted in different lighting and weather conditions. Such distortions reduce the accuracy of the measurement and, in turn, the performance of the vehicle detection algorithms. So, removing a perspective effect with high accuracy is one of the most important tasks that should be handled for later processes.

The aim of the present work is to provide a step forward in the field of ITS, in two directions: (1) providing a low-cost application based on monocular camera for vehicle detection under different weather conditions, urban and interurban areas, and (2) increasing the vehicle detection accuracy, using the MIPM method which plays a key role in the ITS.

State of the art

Investigation of vehicle detection methods based on video camera began in the late 1970s. The monocular camera offers a better trade-off between cost-effectiveness, reliability, and flexibility. Therefore, it is usually preferred for vehicle detection methods (Nastaran Yaghoobi Ershadi and José Manuel Menéndez 2017; Ershadi, Menéndez, and Jiménez 2017; Satzoda et al. 2014).

In any image acquisition process, an innate perspective effect exists. There are many advantages from the removal of this effect in road scenarios, such as better detection of vehicles and lanes in the scene, to find speed and position of the vehicles without distortion or any other Advanced Driver Assistance Systems (ADAS) related applications. Therefore, removing a perspective effect with high accuracy is one of the most important tasks that should be handled.

This effect can be removed by an inverse transformation typically known as Inverse Perspective Mapping which gives a birds-eye view of the road ahead.

CONTACT Nastaran Yaghoobi Ershadi n.yaghoobi@alumnos.upm.es E.T.S. Ingenieros de Telecomunicación, Universidad Politécnica de Madrid, Av. Complutense, 30, Madrid 28040, Spain

In this part, we focus on the IPM algorithm and its improvements by researchers over the last decades, since it still presents some limitations when applied on the road.

IPM was originally introduced by Mallot (Hanspeter et al. 1991). However, Bertozzi et al. (Bertozzi, Broggi, and Fascioli 1998) reported that IPM re-sampled non-homogeneously in order to produce a new image that represents the same scene as acquired from a different position. Muad et al. (Muad et al. 2004) used IPM for lane detection task and vehicle navigation development. The Image quality is not good after IPM transformation. Chien et al. (Chien-Chuan and Ming-Shi 2012) presented the Top-View Transformation Model (TVTM) for image coordinate transformation. TVTM transforming a perspective projection image into its corresponding bird's eye vision. However, they did not test the method under different lighting and weather conditions.

Inverse perspective solutions were later introduced as a fast inverse perspective mapping algorithm (FIPMA) used by Jiang et al. (Gang et al. 2000) aiming to reduce the computational cost of IPM. It resulted to be highly influenced by the video quality leading to very different performances. Authors integrated the calculation of the gradient operator in order to determine the lanes by extracting the edge information. Opposite, our proposal takes advantage of the Hough transform, for line extraction. It is quite insensitive to noise, which is a very good feature when working under varying weather conditions. Another inverse mapping strategy uses a fisheye lens (Chin-Teng, Tzu-Kuei, and Yu-Wen 2010). It is called a fisheye lens inverse perspective mapping (FLIPM). The objective of the mapping is to transform the images from the camera into more precise ones avoiding the previous distortion. This allows detecting obstacles by means of the features of the vertical edges on objects obtained from the remapped images. The static information of the remapped images in a frame determines the features used in the searching stage. This is applied to both the profile and temporal IPM difference image. The proposed method works under brighter backgrounds.

Wang et al. (Chuang and Zhong-Ke 2012) used IPM for traffic stream detection and volume calculation. IPM facilitates the elimination of the geometric distortion related to images. Moreover, marking lines were extracted by introducing geometric constraints of the road structure. Then, the traffic stream was calculated through a background difference method fed by the extracted vehicle contours. Nevertheless, the method can`t be applied to different roads and traffic, and non-favorable weather conditions. The performance of the aforementioned methods can be affected by the perspective and the geometric properties of the objects within an image which can have suffered distortions coming from lighting and weather conditions. These reduce the accuracy and performance of the detection algorithms.

Other IPM-based solutions as Daiming et al. (Daiming et al. 2014) proposing an automatic inverse perspective mapping method based on vanishing point suffers from high computational complexity. Authors implement vanishing point detection and the inverse perspective mapping process for each frame in a system able to adapt to the slope and even the (slight) rotation of the main road direction.

This article proposes a vision-based vehicle detection method using a modified inverse perspective mapping that provides real-time traffic information. It takes advantage of removing the perspective from images to accurately detect vehicles under various weather conditions. Other improvements lay on the stability against perspective and background noise, shadows, and lighting transitions, all of which are difficulties conventional vehicle detection methods have to deal with.

In this work, the quantitative results obtained from the accuracy of MIPM, IPM (Bertozzi, Broggi, and Fascioli 1998) and Homography (Criminisi, Reid, and Zisserman 1999") methods are calculated using the area of the vehicles. Then, Proposed MIPM is compared with TVTM (Chien-Chuan and Ming-Shi 2012), classic IPM (Bertozzi, Broggi, and Fascioli 1998), and FLIPM (Chin-Teng, Tzu-Kuei, and Yu-Wen 2010) transformations to prove its superior performance for increasing the vehicle detection accuracy under different weather conditions. Finally, the processing time of the MIPM is compared to the IPM (Bertozzi, Broggi, and Fascioli 1998), and TVTM (Chien-Chuan and Ming-Shi 2012) methods.

On the other hand, weather conditions have a very high impact on system accuracy. Till now, bad weather conditions are seldom tested in vehicle detection methods (ZiYang and Pun-Cheng 2018). Taking Andrea et al. (Bottino et al. 2016), and Mohammad et al. (Alavianmehr et al., 2015), both systems providing information regarding traffic behavior, it can highlight that accuracy under rainy weather conditions is below 85% in the first one; while the second one provides good accuracy under normal weather (97,19%), but bad weather conditions are not considered.

To that end, we compared detection accuracy of the proposed method with the existing vehicle detection methods in the state of the art (Tsai, Hsieh, and Fan 2007), (Mu et al. 2016), (Shen 2007), (Kamkar and Safabakhsh 2016), (Tian et al. 2014), (Chen and Peng 2012), (Bing-Fei and Juang 2012), (Cucchiara, Piccardi, and Mello 2000), and (Wang 2010) which have been tested under different weather conditions as well. Also, the performance of different vehicle detection methods in four key parts, including the CPU, sensor type, resolution, and runtime are compared.

The result shows, our method has high detection accuracy under different weather conditions, whereas the algorithm is simple and time effectiveness. **Moreover, in choosing the different parts of the algorithm the best trade-off between robustness and computational cost accomplished**. In particular, the modified version of the inverse perspective mapping in which the perspective effect is removed with high accuracy is proposed. Therefore, it utilized for the design of a cost-effective method for vehicle detection. Achieved results verified the better performance of our proposed method in front of previous works in vehicle detection under different weather conditions.

This paper is organized as follows: Next section describes the general structure of the proposed vehicle detection method. Then dataset, experimental results, and comparison of the different methods are present. Finally, Conclusions are provided.

General structure of the proposed vehicle detection method

In order to achieve improved performance in terms of accuracy in vehicle detection, first of all, the proposed method (Figure 1) eliminates the perspective effect more accurately by using a newly proposed Modified Inverse Perspective Mapping.Then the system extracts structural information, such as road lines and lanes using Hough transform (Bakker et al. 2008). Next, a binary image is produced using a gaussian mixture model (Yunda et al. 2004), in a way that the road and the moving vehicles can be displayed in black and white colors, respectively (segment vehicles).

As the system has to obtain the vehicle area, shadows must be removed, but when using Gaussian Mixture Models, shadows are usually combined with the vehicle's area becoming a problem. This is caused by the fact that shadows share the same movement patterns as the vehicle; moreover, shadows demonstrate a similar magnitude

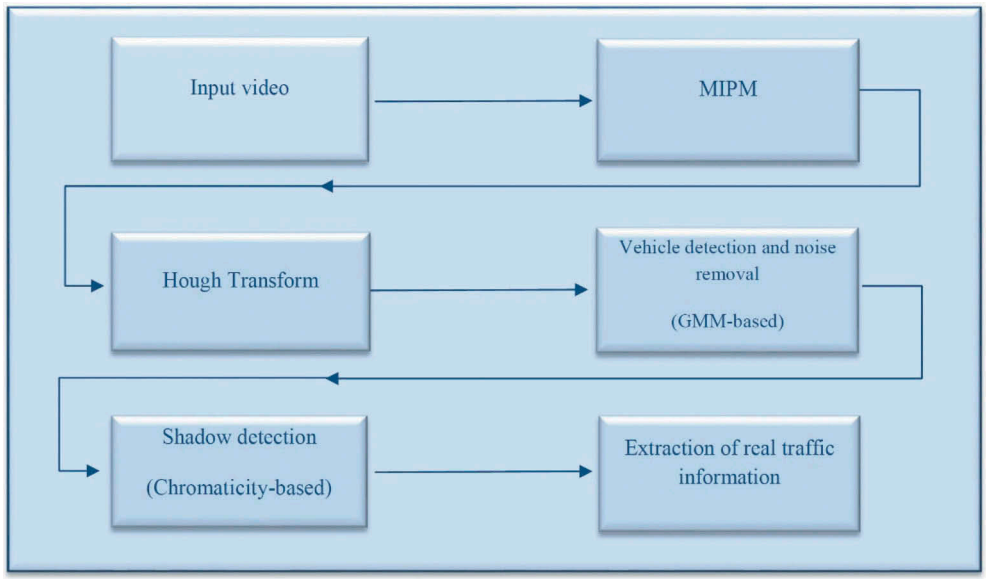

Figure 1. The overall system.

of change in intensity as those of the foreground objects. To overcome this issue, the chromaticity-based method (Yong, Fan, and Runsheng 2007) has been selected (To tackle vehicles shadow effects). Finally, the algorithm extracted the required traffic information, such as speed of vehicles, an area of vehicles (used for classification purposes), types of movement with respect to the structural information of the road and the distance between vehicles. In this way, the vehicles detection ability has been increased. Our overall system structure is illustrated in Figure 1.

Modified inverse perspective mapping

In the last decade, improving the resolution of remapped images and increasing the accuracy of vehicle detection methods are two important topics between researchers. The goal of IPM is removing the perspective effects caused by the camera. IPM affects the geometric properties of subjects in the newly produced image, as it produces a non-homogeneous image which means the image is not regular, and the environment and the vehicle area are not easy to analyze accordingly. In this way, we developed the modified inverse perspective mapping method to achieve better image processing result for vehicle detection and extraction of real traffic information.

In this work, aiming at reducing the classic problem of perspective distortion, a weighting schema proportional to the longitudinal and lateral directions has been used. Once applied, the accuracy of vehicle detection is maximized using simple but effective image processing strategies.

In order to take advantage of the MIPM transform, let $W = \{(x,\ y,\ z)\} \in E^3$ represents the real world coordinate system and $I = \{(u,\ v)\} \in E^2$ be the image-coordinate system. $E^3$and E^2 are three-dimensional (3D) and two-dimensional (2D) Euclidean space, respectively. Considering the flatness of the image, the remapped image is defined as the xy plane of the W space, namely the $S \triangleq \{(x,\ y,\ 0) \in W\}$ surface. Each pixel of the remapped image $\{(x, y, 0) \in W\}$ assigned to $\{(u(x, y, 0),\ v(x, y, 0)) \in I\}$. The coordinate of the camera and viewpoint are defined by $C = (0,\ 0,\ h) \in W$ and $C = (l,\ d,\ h) \in W$, respectively. While the optical axis $\hat{o}$ (viewing direction) defined by the angles $\bar{\theta}$ which is formed between the optical axis $\hat{o}$ and x axis (Figure 2(a)) and, $\bar{\gamma}$ which is formed by the projection (defined by $\hat{\eta}$) of the optical axis $\hat{o}$ on the plane $z = 0$ and the axis x (Figure 2(b)). Also, 2α and $m \times n$ are the aperture angle and resolution of the camera, respectively.

Calibration parameters including intrinsic parameters (camera angular, camera resolution) and extrinsic parameter (viewpoint), which can be determined by measurements.

Image coordinate system to S surface mapping

MIPM uses the mapping from I space to S surface, as the following (1):

$$\begin{cases} x(u,v) = h \times cot\left[\left(\bar{\theta} - \alpha\right) + \frac{u \times 2 \times \alpha}{m}\right] - l \\ y(u,v) = x \times \tan\left[\left(\bar{\gamma} - \alpha\right) + \frac{v \times 2 \times \alpha}{n}\right] - d \\ z(u,v) = 0 \end{cases} \quad (1)$$

Equation (1) returns the point $\{(x, y, 0) \in S\}$ corresponding to point $\{(u, v) \in I\}$. d and $\bar{\gamma}$ are determined by the analysis of the input images as seen in Figure 2. A proper functionality of the system comes from specifying the correct value of the angle θ. As the example, being $\gamma = 90 - \theta$; if γ is too small, only a small area of the road will be transformed in the re-mapped image and if γ is too broad it will overload the system with no necessary information.

S surface to image coordinate system mapping

Transforming the pair (x, y) to u and v as defined in (2) within I surface (Figures 3 and 6). It is clear that images obtained by MIPM are much clearer than images by IPM or other methods as homography. The result is well suited to be used in detection, computation, and calculation of the vehicle area.

$$\begin{cases} u(x,y) = \frac{m}{2 \times a} \times \left(arccot\left[\frac{x+l}{h}\right] - \bar{\theta} + a\right) \\ v(x,y) = \frac{n}{2 \times a} \times \left(\arctan\left[\frac{y+d}{x}\right] - \bar{\gamma} + \alpha\right) \end{cases} \quad (2)$$

Several experiments have been devised to obtain **quantitative results** of the proposed MIPM. **First**, The quantitative results obtained from the accuracy of MIPM, IPM, and Homography methods are

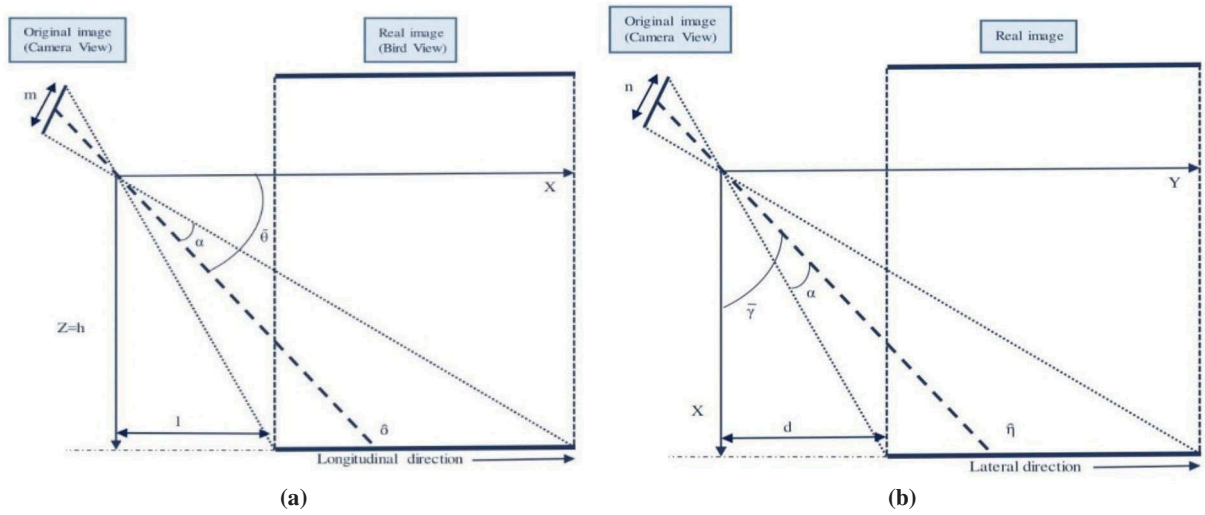

Figure 2. Coordinate system: (a) The *zx* plane; (b) The *xy* plane of the *W* space, namely the *S* surface.

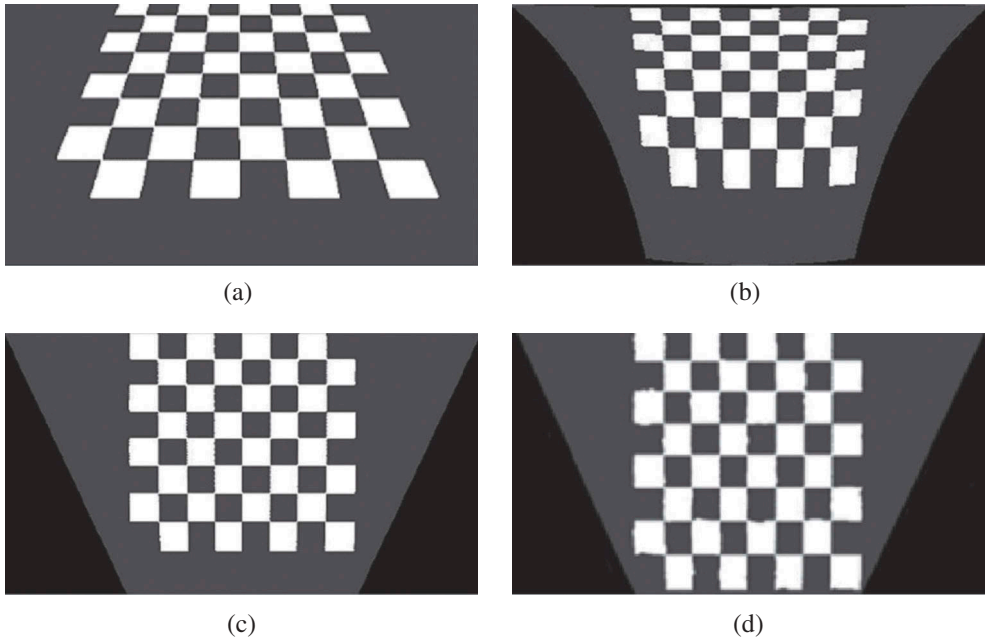

Figure 3. Differences of IPM, MIPM, and Homography methods.
(a) Original image, (b) IPM method, (c) MIPM method, (d) Homography method.

calculated using the area of the vehicles . **Second**, To further evaluate the performance of MIPM, the measured areas of different vehicles in different locations were compared with the reported areas by the manufacture companies (ground truth). **Third**, Proposed MIPM is compared with TVTM (Chien-Chuan and Ming-Shi 2012), classic IPM (Bertozzi, Broggi, and Fascioli 1998) and FLIPM (Chin-Teng, Tzu-Kuei, and Yu-Wen 2010) transformations to prove its superior performance for increasing the vehicle detection accuracy under different weather conditions and show how other different transformation mechanisms affect the vehicle detection accuracy . **Fourth**, The computational performance of the MIPM is compared to the IPM, and TVTM methods .

Qualitative results of MIPM, IPM, and Homography methods is shown with a chess-board. It is placed in a known position in front of the camera, then three different transformations are applied to the image. The difference between the proposed MIPM and the classic IPM can be simply demonstrated in Figure 3. (The camera angle with the horizontal axis is 45 degrees from empirical analysis). Although both IPM and MIPM remove the perspective effect simplifying subsequent calculations, MIPM shows more homogeneous surface than IPM. A further comparison can be done between the MIPM and homography method (Figure 3(d)). The result, applying homography, is not as clear as MIPM.

Moreover, Three methods are applied to the real road images. The examples of transformation results are shown in Figure 6.

Tables 1 and 2 indicate the comparative advantages of MIPM against IPM and Homography methods.

Detection of lanes on the road

The detection of lanes is done by determining local patterns, ideally a point (maximal accumulation), in transformed parameter space (Umbaugh and Scott 1998), in our method by applying the

Table 1. Comparative advantages of MIPM against IPM and homography methods.

The perspective distortion is reduced.
Vehicle detection accuracy is maximized through simple but effective image processing strategies.
The image obtained is much clearer. This clearness makes it feasible to be used in computations and calculation of actual geometrical measurements, such as the vehicle area.
It provides more homogeneous surfaces to be later processed.
Geometric features (of the road) can be easier and more efficiently extracted from the remapped image.

Table 2. Main features of MIPM for vehicle detection.

The area of the vehicle is constant in each location.
The measured distances between vehicles are more accurate.
The measured distances between the vehicle and camera are more accurate.
The measured width of the road and the vehicle is more accurate.

Hough transform. The simplest way of finding these peaks is applying threshold (Hough transform 2019).

The Hough transform is most commonly used for the detection of regular curves such as lines, circles, ellipses, and others. According to Hough Transform, every single pixel in an image space corresponds to a line inside a parameter space. Parameters r and θ are defined in the equation of the line as follows:

$$r = x \times \cos\theta + y \times \sin\theta, \tag{3}$$

which can be rearranged to

$$y = \frac{r - x \times \cos\theta}{\sin\theta}. \tag{4}$$

θ: Theta (radians) is the angle of the line with the range of $-\frac{\pi}{2} \leq \theta \leq +\frac{\pi}{2}$ that indicates the spacing of Hough transform bins along the theta-axis.

r: Rho (pixels) is the distance between the line and the origin that indicates the spacing of the Hough transform bins along the rho-axis.

A relative threshold has been used to extract the unique (r, θ) points relevant to each of the straight lines in our original image: thresholds for local maxima and Gap Allowed (Number of Pixels) are set to 75 and 50, respectively.

Vehicle detection

In many vision systems regarding traffic monitoring, the capability of extracting moving vehicles using a sequence of video is highly crucial and fundamental. To successfully track moving vehicles, classifying them or analyzing the movements, it is very important to perform a detection method both robust and with high accuracy. Detection methods can be categorized into appearance-based methods and motion-based methods.

In turn, appearance-based detection methods are categorized into two groups: (i) feature-based techniques, and (ii) part-based models. In the first group, Scale-Invariant Feature Transform (SIFT) (Chen and Meng 2013), Speeded Up Robust Features (SURF) (Bay, Tuytelaars, and Van Gool 2006), Histogram of Oriented Gradient (HOG) (Khairdoost, Monadjemi, and Jamshidi 2013), and Haar-like features (Viola and Jones 2001) are mostly used for vehicle detection. Specifically, two classes are considered for classification techniques. Popular methods to generate descriptors include Principal Component Analysis (PCA) (Yuan, Sun, and Rui 2016) and Gabor filters (Sun, Bebis, and Miller 2005), among others. The processing speed is slow for the real-time applications (Chen and Meng 2013)(Khairdoost, Monadjemi, and Jamshidi 2013) because SIFT needs to process every keypoints for the vehicle detection (Chen and Meng 2013). While in the second group, a vehicle can be divided into a number of parts modeled by the spatial relation between them (Sivaraman and Trivedi 2013) (Bai, Liu, and Yao 2018). Vehicle detection rates in these methods are lower than ours. Motion-based detection methods are usually categorized into three main groups (i) those using temporal differencing (Li and He 2011), (ii) those analyzing optical flow (Kuo, Pai, and Li 2011), and (iii) those built upon background subtraction (Szwoch and Dalka 2014).

Temporal differencing is by far the most simple method for detection. It can easily adapt to dynamic environments but typically provides poor performances especially in extracting all relevant feature pixels. Optical flow improves the results by means of increasing complexity and computational needs. The majority of optical flow methods cannot be used in full-frame video streams in real-time applications unless specialized high-speed hardware is available. Background subtraction estimates the differences frame by frame of the background evolution and takes advantage of the differences between the current frame and the current background model to detect moving objects. So far, background subtraction has proven to be the category applied most successfully in practice as they can provide the most complete feature data.

Implementation of gaussian mixture model (GMM)

Many applications in the field of image processing rely on efficient and trustworthy background subtraction. Considering the statistical features applied to construct the background model different approaches can be classified. Typical methods proposed in this field use the minimum and maximum values, median values, or take advantage of a single Gaussian or Gaussian Mixture Model (Barcellos et al. 2015), etc. Among subtraction methods, GMM is the most reliable and computationally efficient approach (Zhao and Yi 2017). GMM-based methods require less storage capacity, due to the fact that they do not need to store numerous preceding frames. They are also able to successfully handle gradual lighting changes as they slowly adjust parameters of the Gaussians (Yuhong et al. 2013; Herbon, Tönnies, and Stock 2014). GMM-based methods are capable of handling multimodal distributions caused by real-world application issues such as shadows or, swaying branches. Moreover, GMM responds fast and recovers quickly from backgrounds reappearing in the image. Finally, GMM makes easier the distinction of moving an object by automatically creating a pixel-wise threshold which is generated to flag potential points belonging to estimated moving objects.

GMM is a parametric (Bin, Sun, and Sheng 2017) probability density function. Each pixel in the scene is modeled by a mixture of k Gaussian distributions. The probability of observing the current pixel value is given as follows:

$$P(X_t) = \sum_{i=1}^{k} \omega_{i,t}.\eta(X_t, \mu_{i,t}, \sum i, t), \tag{5}$$

where the probability density for the current guassian is

$$\eta\left(X_t,\ \mu_{i,t},\ \sum i, t\right) = \frac{1}{(2\pi)^{\frac{n}{2}} |\sum i, t|^{\frac{1}{2}}}\ e^{-\frac{1}{2}\left(X_t - \mu_{i,t}\right)\sum_{i,t}^{-1}\left(X_t - \mu_{i,t}\right)} \tag{6}$$

$$\sum_{i=1}^{k} \omega_{i,t} = 1. \tag{7}$$

For simplicity, the covariance matrix is assumed as

$$\sum_{i,t} = \sigma_{i,t}^2 I. \tag{8}$$

And, established as diagonal

$$\sum_{i,t} = diag\left[\sigma_{R_{i,t}}^2, \sigma_{G_{i,t}}^2, \sigma_{B_{i,t}}^2\right] \tag{9}$$

X_t: Pixel value in frame i_t, while t is time
$P(X_t)$: Probability of observing the current pixel value
n: Dimension of the grayscale or RGB color space
k: Number of Gaussian distributions in the mixture
$\mu_{i,t}$: Mean value at time t
$\omega_{i,t}$: Weight associated with the i_{th} gaussian at time t
$\sum i, t$: Covariance matrix
$\sigma_{R_{i,t}}^2, \sigma_{G_{i,t}}^2, \sigma_{B_{i,t}}^2$: RGB variance of GMM component i at time t

Stauffer and Grimson (1999) proposed to set $k = 3$ *to* 5. In the inclement weathers, which include snow, wind, and rain we used $k = 4$ *to* 5, to control the movement of snow, blowing leaves, and so on. Additionally, the experimental results indicate that if $k = 5$ in situations involving low-speed or pause of the vehicles (because of the heavy snow), extracted foreground regions are more clear.

The k Gaussians are ordered following the ratio $\frac{\omega}{\sigma}$. The Background is classified for every Gaussian that is bigger than the designated threshold, and the foreground is classified for the other distribution that is not included in the previous category. The first B Gaussian distributions which exceed a certain threshold T (a fraction between background and foreground distribution) are retained for a background distribution while other distributions are related to the foreground.

$$B = arg\ min_b\left(\sum_{i=1}^{b} \omega_{i,t} > T\right). \tag{10}$$

Note that, T is based on the background scene and the number of components in the Gaussian mixture model. In this work, it was experimentally set to $T = 0,78$.

The values ω, μ, σ are updated as follows if a pixel matched with one of the K Gaussian.

$$\begin{cases} \omega_{k,t+1} = (1-\alpha)\omega_{k,t} + \alpha \\ \mu_{t+1} = (1-\rho)\mu_t + \rho.X_{t+1} \\ \sigma_{t+1}^2 = (1-\rho)\sigma_t^2 + \rho(X_{t+1} - \mu_{t+1}).(X_{t+1} - \mu_{t+1})^T \end{cases}, \tag{11}$$

where

$$\rho = \alpha.\eta\left(X_{t+1}, \mu_{i,t}, \sum i, t\right) \tag{12}$$

α: Predefined learning rate
ρ: Calculated learning rate
$\mu_{i,t}$: Mean
$\sigma_{i,t}^2$: Variance

Slowly background changes require a small learning rate, however, a fast background changes require a larger learning rate. In this work, it was set to α = 0,1.

However, for the unmatched cases, the values are updated as follows:

$$\begin{cases} \omega_{k,\,t+1} = (\,1-\alpha\,)\omega_{k,t} \\ \mu_{\,t+1} = \mu_t \\ \sigma_{t+1}^2 = \sigma_t^2 \end{cases} \tag{13}$$

If it does not match with any of k Gaussian, it is detected as foreground. Therefore, a binary mask is obtained and for the next foreground detection, Gaussian parameters will be updated. Once the parameter maintenance is done, foreground detection can be completed and so on.

In this work, mean and standard deviation are selected as the initial values, which are affected by the extraction of foreground regions. Best results for our complex conditions are obtained with mean value and standard deviation, 349 and 100, respectively. There are some noisy pixels in the foreground regions, thus the morphological operation is used to eliminate the noisy pixels in the foreground regions and reduce disturbance. The example of background subtraction result is shown in Figure 4.

Shadow detection

Shadow detection is an important task for every vehicle detection algorithms. Sometimes, shadows are detected as part of the vehicles in the GMM based-methods as they demonstrate movement patterns that are the same as the moving vehicles and also represent a magnitude of intensity change similar to them.

To overcome this issue, chromaticity-based methods (Sun and Li 2010) sometimes paired with wavelet analysis (Khare, Srivastava, and Khare 2014), texture-based methods (Leone and Distante 2007), geometry-based methods (Chen and Aggarwal 2010), and physical-based methods (Huang and Chen 2009; Martel-Brisson and Zaccarin 2008) have been proposed in the literature. It should be noted that wavelet analysis can decompose the signal into high and low frequencies, but it is not fine to decompose the high frequency (Deng et al. 2017).

In order to have a successful application of chromaticity methods, it is key to choose a color space with a good separation of intensity and chromaticity. The HSI color space can reflect this problem better than other models, such as RGB, YUV, and others (Tsai 2006). The intensity component (I) from HSI color space quantifies the intensity/luminance of the image. The intensity of shadow regions is lower than of vehicles' in the scene. So, the values of I related to pixels in the shadowed

(a) (b)

Figure 4. The result of background subtraction under snowy weather condition.
(a) Original image; (b) After background subtraction.

part, should be lower than those of the pixels in the background. On the other hand, a shadow on the background does not show a change in its hue (H), and if the shadow was cast on a point, the saturation (S) of the point would decrease. This selection provides a better natural separation between luminosity and chromaticity leading to better detection ability in our proposed method (Figure 11). Thus, to detect shadows with the chromaticity-based method, first, RGB color space in the image should be converted to HSI color space. As a result, we assume that; a pixel p is a part of a shadow if the following conditions are satisfied (14).

$$\begin{cases} \beta_1 \le \left(F_p^I / B_p^I\right) \le \beta_2 \\ \left(F_p^s - B_p^s\right) \le \tau s \\ \left|F_p^H - B_p^H\right| \le \tau H \end{cases} \tag{14}$$

F and B: Component values of HSI for the pixel position p in the frame and a background reference image, respectively.

β_1, β_2, τs and τH: Thresholds that were optimized empirically. Multiple values have been tested for several thresholds. The best results in all tested sequences are obtained with values around the following ones: $\beta_1 = 0{,}31$, $\beta_2 = 0{,}57$, $\tau s = 0{,}1$, $\tau H = 0{,}5$.

In some cases, shadow areas separated into shadow pixels or separate regions. Therefore, a connected component analysis has been used to grouping these areas. Afterward, gradient information helps to remove vehicle pixels that were incorrectly selected as a shadow. Using the above equations and differences between the shadow and the vehicle in the images, we extracted boundary for hue, saturation, and intensity (Figure 11).

Dataset and experimental results

The proposed method has been implemented in Matlab. The method is able to process around 10 frames per second on a dual-core processor at 2,5 GHz Intel® Core™ i7 CPU, 16-GB RAM, and 64-bit operating system. A camera has been used for video recording with a frame rate of 30, and a resolution of 576 × 720 pixels.

Datasets

The proposed procedure has been tested with an own generated dataset acquired in Madrid and Tehran. Both video datasets have been recorded along the year (picking samples in different seasons) by collecting information in different hours to then be used for testing the accuracy of the method. More than 80 videos have been collected, with up to 5 min of length in some of them. For a fair evaluation of the proposed method, videos were recorded from different conditions and positions, as follows:

- **Different locations**: The dataset made contains video data collected at different areas from highways, streets, urban and interurban areas **with a variety of vehicles types and colors** (city cars, buses, vans, minivans, pickup trucks, etc.).
- **Various weather conditions**: These conditions were normal, cloudy, sunny, rainy and snowy weathers.
- **Different lighting conditions**: Poor and normal lighting conditions.
- **Traffic density**: Light traffic and regular traffic (assuming no big occlusions due to big trucks and other special vehicles).
- **Different ranges of camera angles, height, and positions**: Different camera angles, height, and positions cause vehicles to have different size, shapes, and orientations in images. The appearance of a vehicle can vary depending on the distance between the vehicle and the camera.

The results show that the followed strategy has significant effects on complex sequences, and conditions. The simulation results verified the better performance of our method compared to similar works in delectability under different weather conditions, perspective and background noise, shadows, and lighting transitions, all of which are difficulties conventional traffic detection methods have to deal with. Figure 5 shows some examples of the recorded dataset from different positions, locations, weather, and lighting conditions.

Experimental results

Experimental results are divided into three parts. The first part is providing the results of different parts of the solution. The second part presents the evaluation of the performance of the proposed method. Then, the last part provides information regarding the computational complexity and processing time of the proposed method.

Results of the working blocks of the proposed vehicle detection method

Modified inverse perspective mapping. The proposed approach was tested several times in real road scenarios. The qualitative results obtained from the MIPM, IPM, and Homography methods are illustrated in Figure 6. Using MIPM to remap the images, geometric features of the road can be easier and more efficiently extracted from the remapped image compared to classic IPM and Homography methods.

The performance of the proposed MIPM is compared with the standard IPM and Homography methods. Different types of vehicles in different locations and conditions were randomly selected. Then, MIPM, IPM and Homography methods are applied to the images. Using GMM and chromaticity-based method we segmented the vehicles and removed the shadows. Finally, the vehicles areas were calculated.

In this paper, the area of the vehicles is used as a measure to evaluate the performance of IPM, homography, and MIPM. So, Equation 15 is used to normalize the vehicle's area. In summary, the area of the vehicle is compared to the first frame.

$$\text{Area Normalization} = \frac{\text{Area of vehicle}}{\text{Base area of vehicle}} \tag{15}$$

The computed area of the vehicle in increasing frames, using MIPM, IPM, and Homography, is shown in Figure 7.

MIPM performance is similar to IPM and Homography methods in the first frames, but it is different in the following ones. Variations of the vehicle area along with its direction show that MIPM is not only able to successfully remove perspective with a suitable scale, it can also create better estimations for the moving objects. As the results indicated our MIPM is more accurate than IPM and Homography methods.

Hence, it can be inferred that MIPM outperforms IPM and Homography methods as aforementioned in Table 2.

To further evaluate the performance of MIPM, the measured areas of different vehicles in different locations were compared with the reported areas by the manufacture companies (ground truth). Accordingly, every square millimeter was considered as a pixel; then, Equation 15 was applied to normalize the results. Considering the position and direction of the vehicles, we

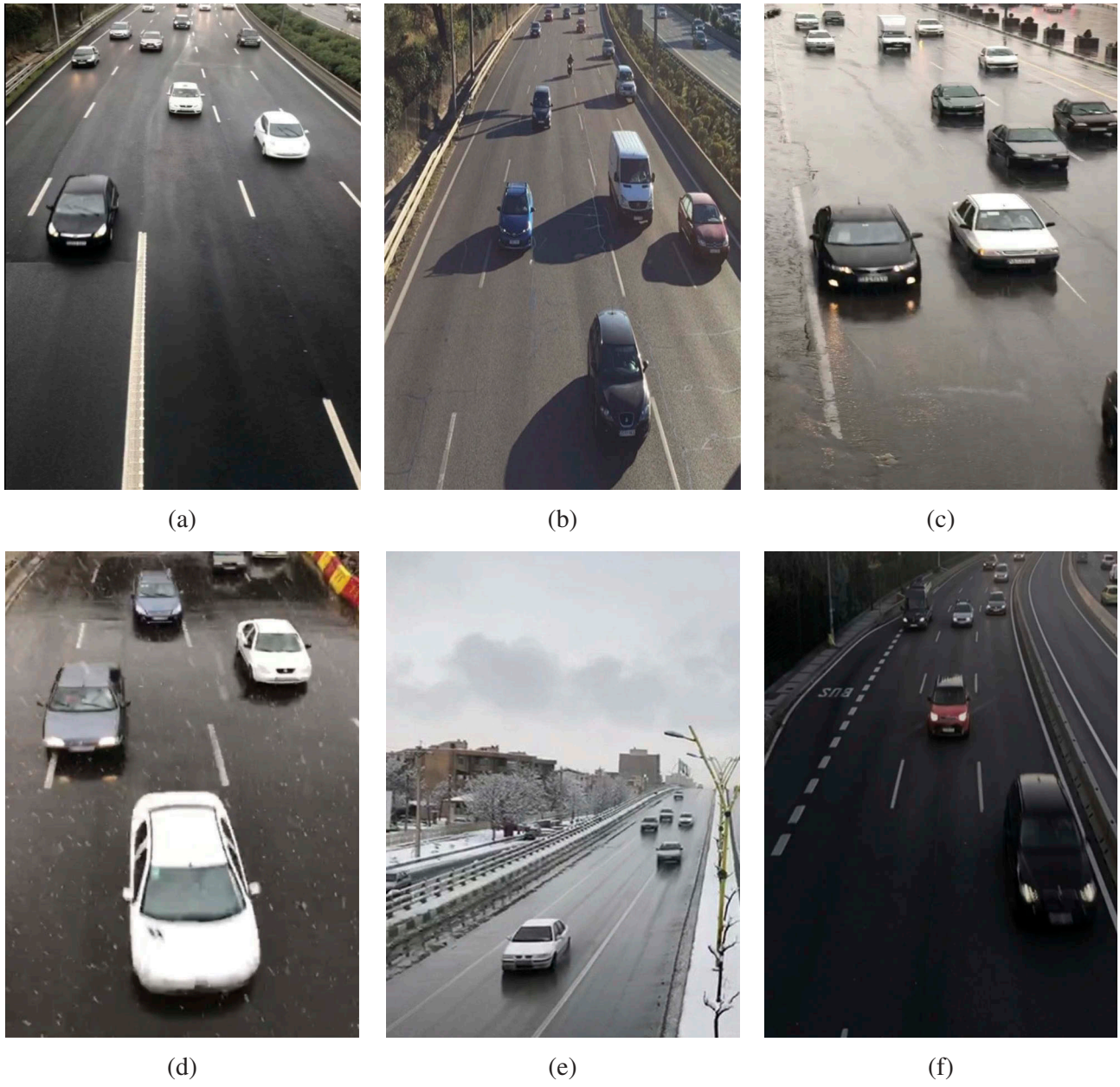

Figure 5. The recorded dataset in Madrid and Tehran.

(a) Normal weather, the camera is located in the center of the bridge on an urban area. (b) Sunny weather, the camera is located in the center of the bridge on an urban area. (c) Rainy weather, the camera is located on the left side of the bridge on an interurban area. (d) Snowy weather, the camera is located in the center of the bridge on a highway. (e) Cloudy weather, the camera is located on the right side of the bridge on an interurban area. (f) Low lighting condition, the camera is located in the center of the bridge on a highway.

measured the vehicle's area (cm) in the images and compared them with actual areas. The results relating to one of the vehicles is illustrated in Figure 8.

Results indicate that areas measured using the proposed MIPM method are closer to the actual ones in the 90% of the tested vehicles (compared to real areas with $R^2 > 0.98$).

As quantitive and qualitative results indicated, image qualities after IPM and Homography methods are lower than MIPM. The elimination of the perspective effect is done with more accuracy, allowing much more efficient and robust vehicle detection implementation.

Locating lane areas. To locate the lane areas in the images, Hough transform has been used due to its structure and performance to detect the white marks determining the lines inside the road images. The accuracy for line detection is calculated in overlap with ground truth. This is usually generated by marking the individual lane marker locations in images.

In this paper, to extract local maxima or bright points, the system takes advantage of the accumulator array thresholding, then some thinning is applied to the isolated clusters of bright points in the accumulator array image. Local maxima whose values were equal or greater than some fixed percentage of the global maximum value are considered. An accumulator covering the hough space is used to determine the areas where most Hough space lines intersect.

Figure 9(b,c) demonstrates how Hough transform can deal with lane detection. In this figure, lines are not straight, but Hough

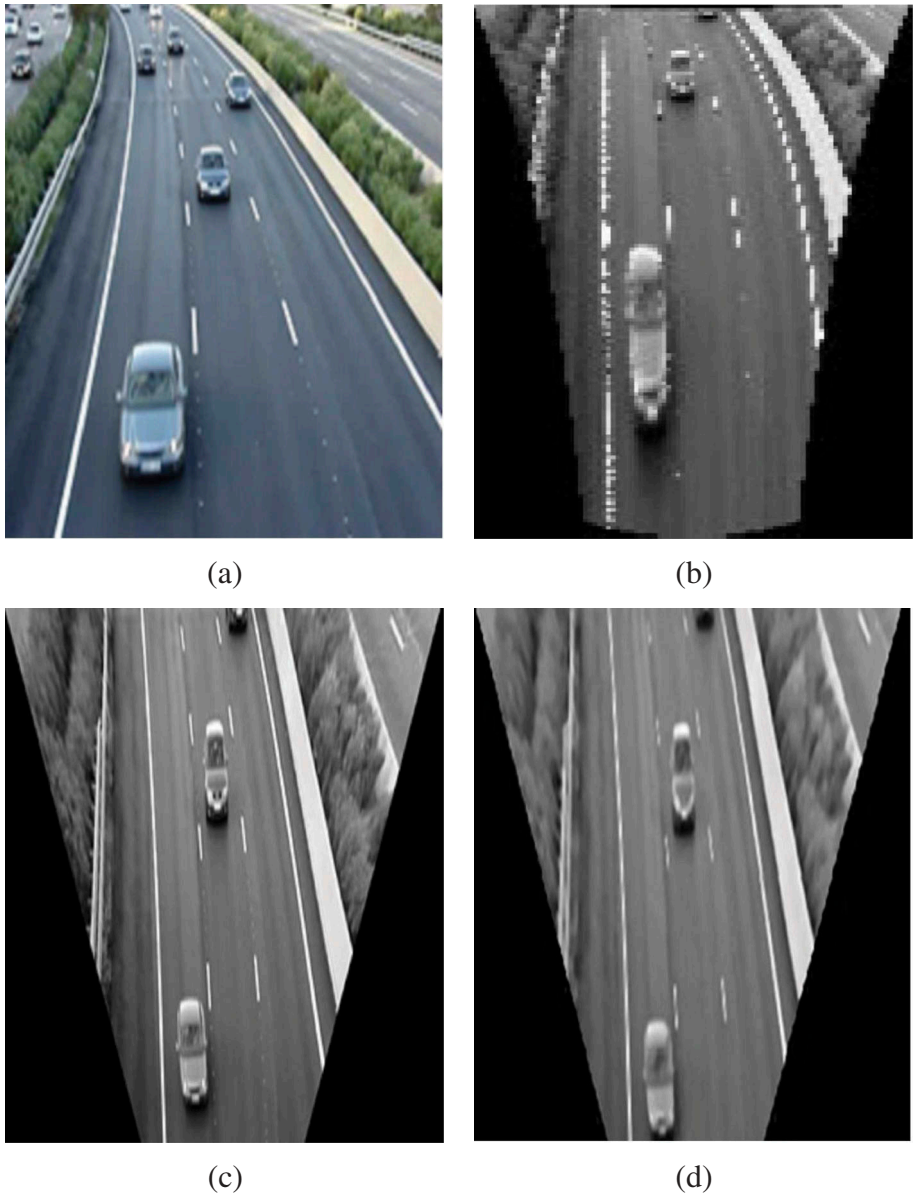

Figure 6. The qualitative results of the remapped image. (a) Original image with perspective effect (b) Remapped image that removed perspective with IPM (c) Remapped image that removed perspective with MIPM (d) Remapped image with Homography method.

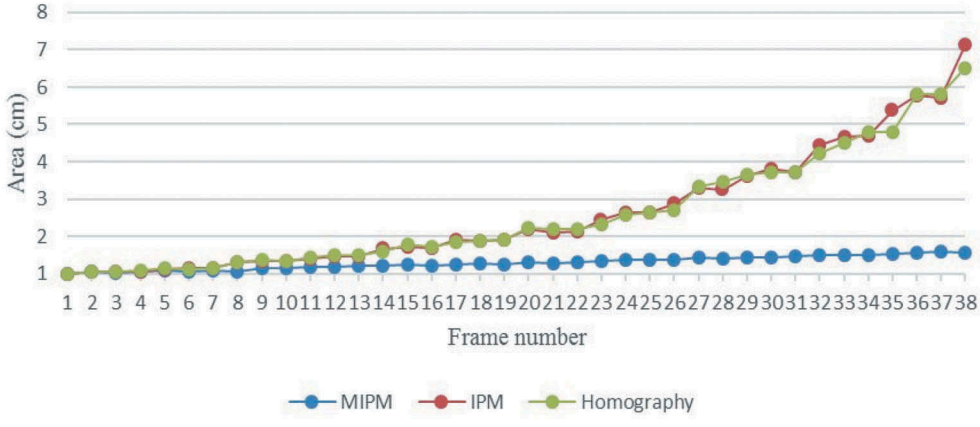

Figure 7. Comparison of the vehicle area variation along with its direction using three methods.

Figure 8. Comparison of the actual vehicle's area and the obtained area from image considering the position and direction of the vehicle.

transform can be also applied for curve detection if the location of a boundary is known, in which its shape can be described as a parametric curve (e.g. a straight line or conic). The results will not be affected by gaps in curves, neither by the noise. As shown in Figure 9(d–f) road lines were chosen to define lane areas.

Vehicles detection. Figure 10 shows the detection of a vehicle in lane one of the highway in consecutive frames. The results indicate that, after applying MIPM, the system can extract real properties of the vehicles such as area, width, length as well as the distance between the vehicles with more accuracy.

However, to improve the results, it is much better to remove noise from images (such as the shadow) detected by GMM.

Shadow removing. Many researchers work with HSV (Hue, Saturation, Value) color space for shadow detection or removing. However, our proposed method works on HSI color space. The result of the shadow removing is shown in Figure 11.

To validate the selection of the solution working with HSI color space some comparisons with other methods have been carried out. In this paper, shadow detection performance has been evaluated using two ratios: shadow detection rate (η) and shadow discrimination rate (ε) (16) as follows (Sanin, Conrad Sanderson, and Lovell 2012):

$$\begin{cases} \eta = \frac{TP_S}{TP_S + FN_S} \\ \varepsilon = \frac{TP_F}{TP_F + FN_F} \end{cases} \tag{16}$$

where TP_S, FN_S, TP_F, *and* FN_F, respectively, indicate the true positive area of shadow, the false negative area of shadow, the true positive area of foreground and the false negative area of the foreground. The shadow detection rate (η) is concerned with labeling the maximum number of cast shadow pixels as shadows. However, the shadow discrimination rate (ε) is concerned with maintaining the pixels that belong to the moving object as foreground.

The comparison has been done through 45 frames that were selected randomly from the recorded datasets in different weather conditions and locations. The average values of (η), (ε) and average processing time per frame are calculated for the comparing results between three kinds of shadow detection methods in Table 3.

As the result indicated, the chromaticity-based method with HSI color space is able to achieve both high detection and discrimination rates even under bad weather conditions. Also, it is fast and simple. We observed that when vehicles are darker and have similar colors to the background the probability of failure increases.

The geometry-based method fails in more cases when the shadows have the same orientations as the vehicles. The texture-based method fails for pixels located in a non-textured background and requires extra steps to calculate the gradients. So, it needs a higher computational time. In conclusion, our selected solution provides the best performance overall.

Geometric center. Once a vehicle is detected, to obtain the position on the road, the geometric center needs to be determined, as shown in Figure 12(a–b). The geometric center of a vehicle has been found by means of 'regionprops' and 'centroid' functions in MATLAB. Then, each geometric center is considered as a vehicle in consecutive frames, Figure 12(c). Moreover, the path of a vehicle can be obtained by aligning its geometric centers in consecutive frames, Figure 12(d).

Quantitative evaluation

The performance of the complete proposed method was evaluated on the randomly selected frames from the recorded dataset. The detection accuracy can be affected by different weather conditions and road positions. Thus, 100 samples (each sample consists of one frame) were selected randomly from different environments for each category.

The generation of the contents for the comparison was done by labeling the vehicles manually in the datasets (Ground Truth), then from the randomly selected frames for the test, the detection rate was obtained by comparing with the labeled data of these frames. For evaluation the method four parameters are defined as follows:

- True Positives (TP): Number of the correctly detected vehicles by the method.
- False Positives (FP): Number of the detected objects (non-vehicles) in the background that is incorrectly classified as vehicles.
- False Negatives (FN): Number of vehicles that were missed by the method.
- True Negatives (TN): The situation that does not exist neither in the ground truths nor the result (correctly rejected). The non-vehicles present in neither the GT nor the system under test. Such as a human, a motorbike or a bicycle.

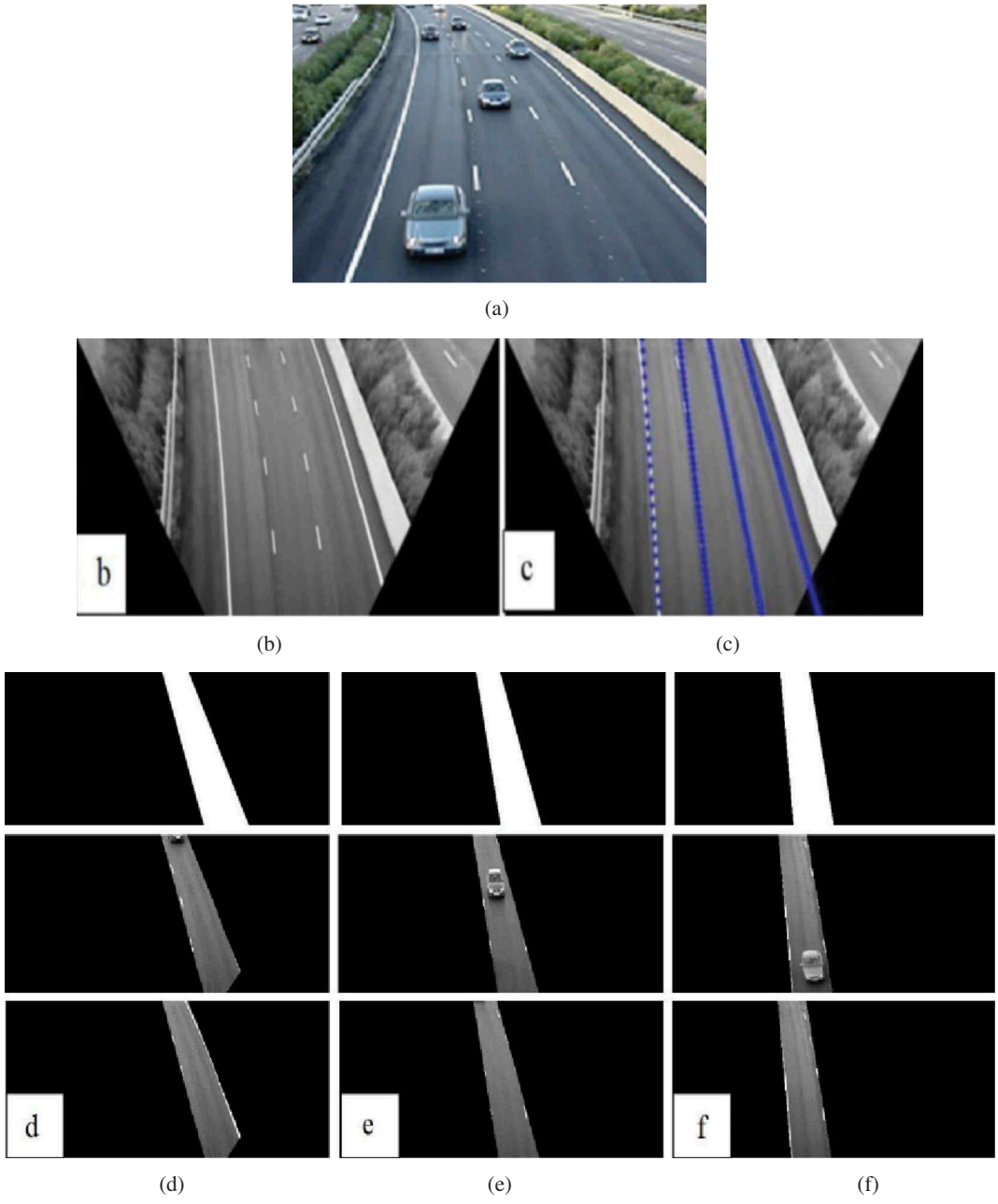

Figure 9. (a) Original image (b) Removed perspective with MIPM (c) Detected lines (d) lane1 (e) lane2 (f) lane3.

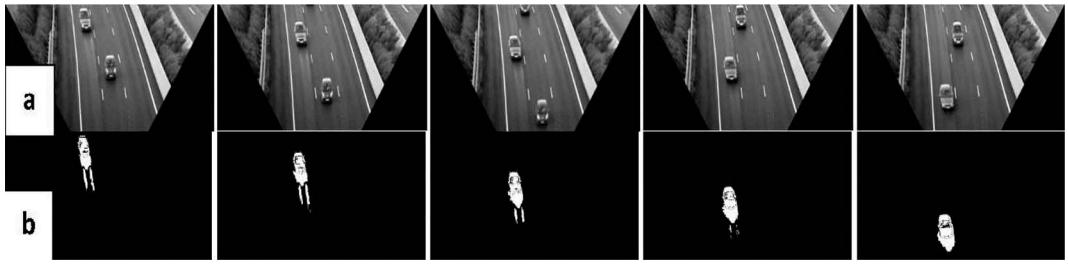

Figure 10. Detection of the vehicle in lane 1 of the high way.
(a) Remapped by MIPM (b) Detected vehicle in lane 1 by GMM.

Additionally, Ground Truth (GT) is defined as $GT = TP + FN$.

Then, the performance of the complete method is evaluated by several metrics as follows:

- **True Positive Rate (TPR)** is the percentage of correct vehicles that are detected. It is also called as a **sensitivity of the system, Detection Rate (DR),** or **Recall.**

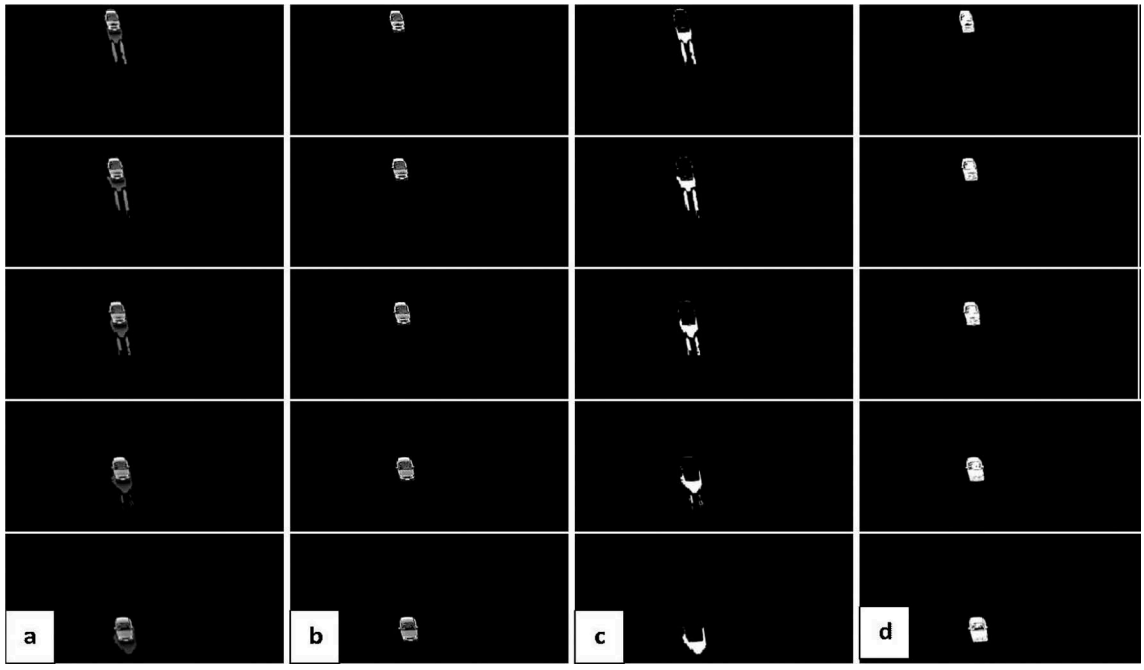

Figure 11. Shadow removing in HSI color space.

(a) Results of the dot product between original images and binary images; (b) After shadow removing in the original images; (c) Shadow detection; (d) Results of the difference between the shadow images and the binary ones.

Table 3. Comparison of shadow detection methods.

Methods	Chromaticity based method with HSI color space	Texture based method Shoaib, Dragon, and Ostermann (2009)	Geometry-based method Hsieh et al. (2003)
$\eta(\%)$	97,58	81,39	73,95
$\varepsilon(\%)$	98,72	90,23	79,63
Time (ms/f)	7,21	87,48	12,52

$$TPR = \frac{(TP)}{(TP + FN)} \times 100 \tag{17}$$

- **False Alarm Rate (FAR)** is the percentage of non-vehicles that are detected.

$$FAR = \frac{(FP)}{(FP + TP)} \times 100 \tag{18}$$

- **Precision** and **Accuracy (ACC)** of the method can be calculated as follows:

$$Precision = \frac{TP}{TP + FP} \times 100 \tag{19}$$

$$ACC = \frac{(TP + TN)}{(TP + FN + FP + TN)} \times 100 \tag{20}$$

Precision is the percentage of detected vehicles that are correct. However, accuracy is the percentage of the actual performance of the method with regard to both correctly detecting and correctly rejecting.

The evaluation is divided into **three** parts:

First, the performance of the complete proposed method was evaluated on the randomly selected frames from the recorded videos. Quantitative evaluation of the performance of the proposed method under different conditions is shown in Table 4. This table was evaluated for vehicle counting. The number of detected vehicles by the proposed method, True Positive Rate, False Alarm Rate, precision, and Accuracy are considered.

The method, under normal and cloudy weather conditions, has very high True Positive rates with 99.52% and 99.44%, respectively. The frames on these conditions are clear. False positives have occurred in a few cases, due to the cluttered areas of the urban roads. Some objects in the scene were detected as a vehicle which affected the detection accuracy.

Under bad weather conditions, the vehicles move more slowly (due to no field of view for a driver) comparing with normal weather. So, if there is a big vehicle or an occlusion in the scene, it takes a long time for them to leave the scene (i.e. vehicle behind a truck for a long period of time cannot be detected). Thus, randomly selected sequences will decrease the detection rate under such conditions. Moreover, missed detections were occurred due to the noise and blurred image sequences in the far distance from the camera. Our proposed method shows 95.39% detection rate under rainy weather conditions, while under snowy and low lighting conditions have better TPR with 98.60% and 97.65%, respectively. Also, in a few cases, the method failed to detect the white vehicles in snowy weather conditions very far from the camera. It is able to detect more than 98.23% of the vehicles in all the tested sequences in the different weather and lighting conditions. In conclusion, the method that was proposed in the previous section can provide a robust solution to monocular-based vehicle detection. Figure 13 shows the detection results of the proposed method. Additionally, the results show that the proposed method can achieve close to real-time performance.

Second, Generally, each proposed inverse perspective mapping methods has different transformation mechanisms. Proposed MIPM is compared with TVTM (Chien-Chuan and Ming-Shi 2012), classic IPM (Bertozzi, Broggi, and Fascioli 1998), and FLIPM (Chin-Teng, Tzu-Kuei, and Yu-Wen 2010) transformations

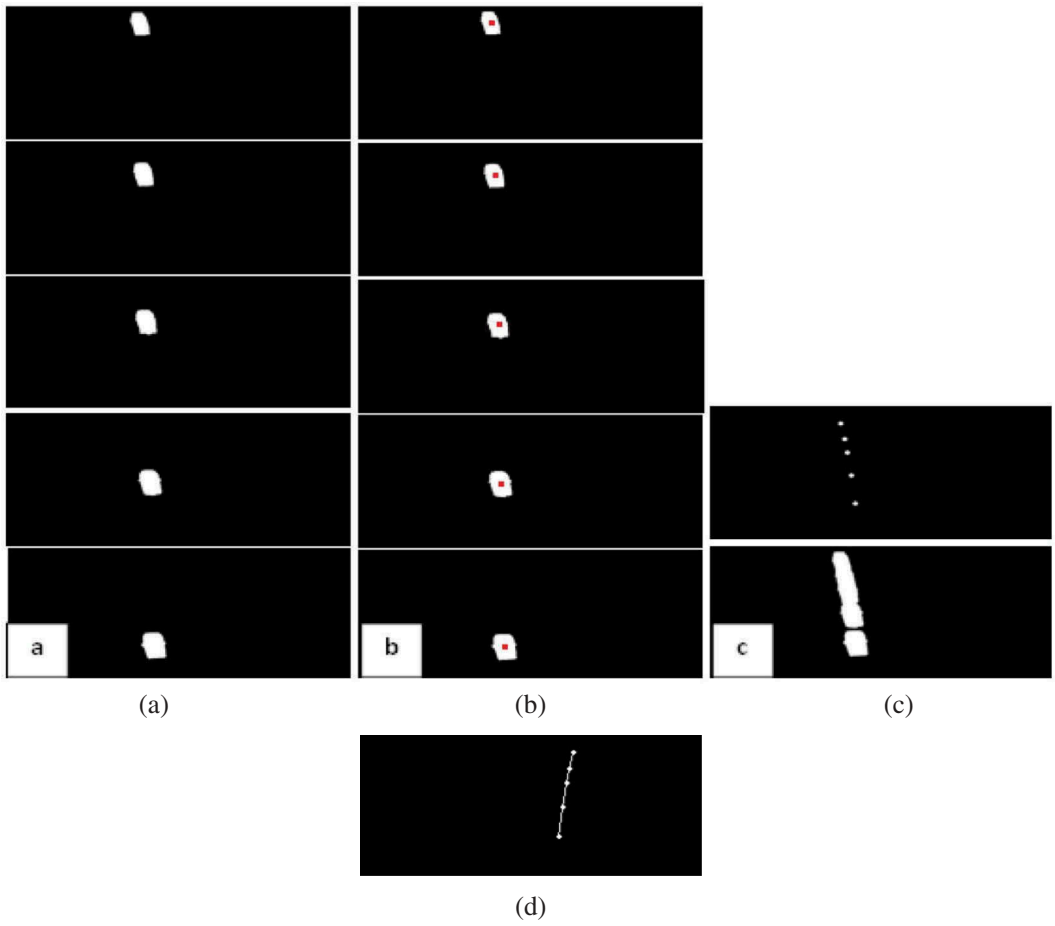

Figure 12. Geometric center.

(a) Binary images (b) Geometric centers (red points) (c) Aligning the geometric centers (white points)(d) Path of the vehicle (path tracking by frame-by-frame evaluation of blobs centers)

Table 4. Evaluation of the proposed method, under different conditions.

Category	GT	TP	FP	FN	TPR%	FAR%	Precision%	ACC%
Normal weather	628	625	9	3	99.52	1.41	98.58	98.12
Sunny weather	507	501	13	6	98.81	2.52	97.47	96.36
Cloudy weather	539	536	10	3	99.44	1.83	98.16	97.64
Rainy weather	478	456	41	22	95.39	8.24	91.75	87.93
Snowy weather	357	352	9	5	98.60	2.49	97.50	96.20
Low lighting condition	383	374	24	9	97.65	6.03	93.96	91.95

to prove its superior performance for increasing the vehicle detection accuracy under different weather conditions and show how other different transformation mechanisms affect the vehicle detection accuracy. It should be noted that the same evaluation criteria were applied to all methods. Identically, 100 samples were selected randomly from different locations and conditions to make the comparison. The comparison results are shown in Tables (5–8).

From the results obtained, the proposed MIPM method is of better clarity and transparency compared with the IPM, Homography, and other methods. As the results indicated, the removal of the perspective effect with high accuracy (MIPM), increases the detection rate of the method. The performance of the method is decreased under all transformation methods as the noise level increases.

The image quality is not good after IPM (Bertozzi, Broggi, and Fascioli 1998) transformation. In this way, FAR increases under all tested conditions compared with using MIPM in the proposed vehicle detection method. The detection rate of the method with IPM transformation is decreased to 96,44%, 92,67%, 96,07% and, 95,03% under sunny, rainy, snowy and low lighting conditions, respectively. The TVTM (Chien-Chuan and Ming-Shi 2012) produced good result just under specific conditions as camera tilt angle θ =45° with yaw angle $\gamma = 0$. Thus, this method makes difficult to produce clear images under different camera positions. Overall, the average accuracy of the proposed method decreases with TVTM transformation. In (Chin-Teng, Tzu-Kuei, and Yu-Wen 2010) the authors did not report the detection accuracy by their proposed transformation and similarity of the original image and remapped one. As results indicate, the proposed transformation mechanism decreases the vehicle detection accuracy, thus, false negative and positive rates have increased.

In sum, a comparative study of the IPM (Bertozzi, Broggi, and Fascioli 1998), TVTM (Chien-Chuan and Ming-Shi 2012), and FLIPM (Chin-Teng, Tzu-Kuei, and Yu-Wen 2010) against the MIPM shows that the accuracy of the proposed vehicle detection method using MIPM is much more higher than other transformation methods under different weather conditions.

Third, we aim to compare the performance of the proposed method with other vehicle detection methods in the state of the art which have been tested under different weather conditions as well. Table 9 is considering the TPR of the different methods and comparing with our method under unfavorable weather conditions.

The results confirmed that our method is providing the highest detection rates in front of other published methods in almost all weather conditions.

Figure 13. Vehicles detection under different weather conditions and locations using our MIPM method (a-f).

Table 5. Comparison of the performance of the MIPM in front of other transformation methods under sunny weather conditions.

	GT	TPR%	FAR%	Precision%	ACC%
TVTM (Chien-Chuan and Ming-Shi 2012)	507	97.23	3.33	96.66	94.11
IPM (Bertozzi, Broggi, and Fascioli 1998)	507	96.44	4.30	95.69	92.48
FLIPM (Chin-Teng, Tzu-Kuei, and Yu-Wen 2010)	507	98.22	2.92	97.07	95.42
MIPM	507	98.81	2.52	97.47	96.36

Table 6. Comparison of the performance of the MIPM in front of other transformation methods under rainy weather conditions.

	GT	TPR%	FAR%	Precision%	ACC%
TVTM (Chien-Chuan and Ming-Shi 2012)	478	93.51	9.33	90.66	85.38
IPM (Bertozzi, Broggi, and Fascioli 1998)	478	92.67	10.68	89.31	83.52
FLIPM (Chin-Teng, Tzu-Kuei, and Yu-Wen 2010)	478	94.14	8.90	91.09	85.71
MIPM	478	95.39	8.24	91.75	87.93

Table 7. Comparison of the performance of the MIPM in front of other transformation methods under snowy weather conditions.

	GT	TPR%	FAR%	Precision%	ACC%
TVTM (Chien-Chuan and Ming-Shi 2012)	357	96.91	4.15	95.84	93.06
IPM (Bertozzi, Broggi, and Fascioli 1998)	357	96.07	5.24	94.75	91.29
FLIPM (Chin-Teng, Tzu-Kuei, and Yu-Wen 2010)	357	97.75	3.05	96.94	94.87
MIPM	357	98.60	2.49	97.50	96.20

Table 8. Comparison of the performance of the MIPM in front of other transformation methods under low lighting conditions.

	GT	TPR%	FAR%	Precision%	ACC%
TVTM (Chien-Chuan and Ming-Shi 2012)	383	95.82	6.85	93.14	89.58
IPM (Bertozzi, Broggi, and Fascioli 1998)	383	95.03	7.84	92.15	88
FLIPM (Chin-Teng, Tzu-Kuei, and Yu-Wen 2010)	383	96.60	6.32	93.67	90.75
MIPM	383	97.65	6.03	93.96	91.95

Table 9. Comparison of TPR of the proposed method with other vehicle detection methods under different weather conditions.

Weather conditions	Tsai, Hsieh, and Fan (2007)	Mu et al. (2016)	Shen (2007)	Kamkar and (Safabakhsh 2016)	Tian et al. (2014)	Chen and Peng (2012)	Bing-Fei and Juang (2012)	Cucchiara, Piccardi, and Mello (2000)	Wang (2010)	Proposed method
Sunny	-	-	-	74.82%	94.3%	-	97,55	97,8	98,5	**98,81%**
Cloudy	93.1%	83.7%	-	-	97.9%	-	97,35	97,6	99,2	**99,44%**
Rainy	94.6%	74.6%	**95.8%**	94.5%	93.8%	71%	85,9	91,5	94,2	95,39%
Snowy	-	72.2%	-	-	-	-	-	-	-	**98,60%**
Low lighting	-	-	83.3%	85.06%	94.5%	76%	82,1	78,6	89,2	**97,65%**

In this work, the testing sequences were curated to finally discarding sequences containing too many occlusions (e.g. vehicles occluded by a front larger one) and the ones with poor resolution (e.g. blurred due to bad weather conditions and along distances of vehicles from the camera or badly marked lanes).

Computational complexity

In this section, the computational complexity of the proposed method is discussed, by clarifying the amount of time required. It is a low-cost system, by considering that the single camera is used instead of more expensive devices such as radars, lidars or stereo cameras, and in the other hand, it avoids costful deployments as the one needed to install magnetic loops and piezo-electric sensors. The computational requirement of MIPM operation depends on the projected pixels, which in turn depends on the camera view angle. If θ is small, the amount of the road pixel will decrease, and sky region will be discarded from the Region Of Interest (ROI).

Regarding the processing times, the performance of MIPM is compared with the IPM (Bertozzi, Broggi, and Fascioli 1998), and TVTM (Chien-Chuan and Ming-Shi 2012) methods. One hundred frames were selected randomly from different locations and conditions, and then the average transformation time for each method was calculated.

The average processing time of the MIPM method is 53,71 ms/f. Using 240×320 instead of 576×720 pixels would result in a reduction of processing time in close to 50%. MIPM takes about 53% of the total processing time as it is the main core of the proposed method.

However, the average processing time of the IPM and TVTM methods are 76,9 ms/f and 119 ms/f, respectively. It should be noted that, for the fair evaluation of the comparison, the same image pixels were used for all tested methods.

The average processing time of the proposed vehicle detection method is 100 ms/f. The selected size of ROI for the recorded videos can decrease (or increase) the computational time of vehicle detection method.

The proposed MIPM is less time-consuming. Even classical IPM that produces several artifacts on the resultant image (Figure 6), leading to a reduction of the effectiveness of the vehicle detection method needs a longer time to be calculated.

Table 10 exhibits the performance of different vehicle detection methods. We presented compared results in four topics, including the CPU, sensor type, resolution, and runtime reported by each method.

One of the main advantages of the proposed vehicle detection method is its simplicity. It is a computationally inexpensive method and can be used for real-time applications like counting the number of vehicles. In terms of time consumption and efficiency, it is less time-consuming and has a higher detection rate, outperforming others. Moreover, it is proved to be able to eliminate the perspective effect more accurately.

Conclusions

In this paper, a robust algorithm to eliminate the perspective effect in traffic images is proposed. MIPM is able to produce an image

Table 10. Comparisons of the computational performance of vehicle detection methods.

Methods	Proposed method	Tsai, Hsieh, and Fan (2007)	Kamkar and Safabakhsh (2016)	Cucchiara, Piccardi, and Mello (2000)	Niknejad et al. (2012)	Ohn-Bar and Trivedi (2015)
CPU (GHz)	2.5	2.4	3.6	N/A	3.0	3.0
Sensor Type	Single camera	Single Camera	Single Camera	Single camera	Single camera	Single camera
Resolution (pixels)	576×720	N/A	N/A	N/A	640×480	1242×375
Runtime (ms/f)	100	500	200	200	500	200

from the original picture without any harmful effect on it. Thus, it is capable to extract real traffic information more accurately. We have applied this method to increases the accuracy of vehicle detection method under different conditions. A complete dataset of own recorded videos from different environments under varying weather conditions has been built. The sequences were used to evaluate the robustness and efficiency of the proposed vehicle detection method. Then, further calculations have been done to obtain both qualitative and quantitative results. Experimental results proof higher accuracy when using transformed images by MIPM leading to an increasing vehicle detection performance.

Comparing results indicate that MIPM was not only simple and straightforward, but it was also more accurate in front of previously published methods. Additionally, results show that the proposed approach is computed in less time than other previous works in this filed. In sum, the proposed method is able to solve the significant problem of accurate and real-time vehicle detection under different weather conditions, especially when these are bad.

Disclosure statement

No potential conflict of interest was reported by the authors.

ORCID

Nastaran Yaghoobi Ershadi http://orcid.org/0000-0002-1112-2068
José Manuel Menéndez http://orcid.org/0000-0003-0584-2250
David Jiménez Bermejo http://orcid.org/0000-0002-7382-4276

References

Agarwal, V., N. V. Murali, and C. Chandramouli. 2009. "A Cost-Effective Ultrasonic Sensor-Based Driver Assistance System for Congested Traffic Condition." *IEEE Transactions on Intelligent Transportation System* 10: 486–498. doi:10.1109/TITS.2009.2026671.

Alavianmehr, M. A., A. Zahmatkesh, and A. Sodagaran. 2015. "A New Vehicle Detect Method Based on Gaussian Mixture Model along with Estimate Moment Velocity Using Optical Flow." The 14th International Conference on Traffic and Transportation Engineering (ICTTE), Tehran, Iran.

Bai, S., Z. Liu, and C. Yao. 2018. "Classify Vehicles in Traffic Scene Images with Deformable Part-Based Models." *Machine Vision and Applications* 29: 393–403. doi:10.1007/s00138-017-0890-y.

Bakker, T., H. Wouters, A. Kees V., J. Bontsema, L. Tang, and J. Müller. 2008. "A Vision Based Row Detection System for Sugar Beet." *Computers and Electronics in Agriculture* 60 (1): 87–95. doi:10.1016/j.compag.2007.07.006.

Barcellos, P., C. Bouvié, F. L. Escouto, and J. Scharcanski. 2015. "A Novel Video Based System for Detecting and Counting Vehicles at User-Defined Virtual Loops." *Expert Systems with Applications* 42 (4): 1845–1856. doi:10.1016/j.eswa.2014.09.045.

Bay, H., T. Tuytelaars, and L. Van Gool. 2006. "Surf: Speeded up Robust Features." In Computer vision (ECCV), Jan, 404–417. Berlin Heidelberg.

Bertozzi, M., A. Broggi, and A. Fascioli. 1998. "Stereo Inverse Perspective Mapping: Theory and Applications." *Image and Vision Computing* 16 (8): 585–590. doi:10.1016/S0262-8856(97)00093-0.

Bottino, A., A. Garbo, C. Loiacono, and S. Quer. 2016. "Street Viewer: An Autonomous Vision Based Traffic Tracking System." *Sensors* 16. doi:10.3390/s16122100.

Bugdol, M., Z. Segiet, and M. Krecichwost. 2014. "Vehicle Detection System Using Magnetic Sensors." *Transport Problems* 9 (1): 49–60.

Celik, T., and H. Kusetogullari. 2010. "Solar-Powered Automated Road Surveillance System for Speed Violation Detection." *IEEE Transactions on Industrial Electronics* 57 (9): 3216–3227. doi:10.1109/TIE.2009.2038395.

Cevher, V., R. Chellappa, and J. H. McClellan. 2009. "Vehicle Speed Estimation Using Acoustic Wave Patterns." *IEEE Transaction on Signal Process* 57 (1): 30–47. doi:10.1109/TSP.2008.2005750.

Chen, -C.-C., and J. Aggarwal. 2010. "Human Shadow Removal with Unknown Light Source." International Conference on Pattern Recognition, 2407–2410. Istanbul, Turkey.

Chen, D. Y., and Y. J. Peng. 2012. "Frequency-Tuned Taillight-Based Nighttime Vehicle Braking Warning System." *IEEE Sensors Journal* 12 (11): 3285–3292. doi:10.1109/JSEN.2012.2212971.

Chen, X., and Q. Meng. 2013. "Vehicle Detection from UAVs by Using SIFT with Implicit Shape Model." In Proceedings of IEEE International Conference on Systems, Man, and Cybernetics (SMC), Oct, 3139–3144, Manchester, UK.

Chen, Z., N. Pears, M. Freeman, and J. Austin. 2014. "A Gaussian Mixture Model and Support Vector Machine Approach to Vehicle Type and Colour Classification." *IET Intelligent Transportation Systems* 8: 135–144.

Cheng, J., Z. Xiang, T. Cao, and J. Liu. 2014. "Robust Vehicle Detection Using 3D Lidar under Complex Urban Environment." Robotics and Automation (ICRA), IEEE International Conference, Hong Kong, China.

Chien-Chuan, L., and W. Ming-Shi. 2012. "A Vision Based Top-View Transformation Model for A Vehicle Parking Assistant." *Sensors* 12: page 4431–4446. doi:10.3390/s120404431.

Chin-Teng, L., S. Tzu-Kuei, and S. Yu-Wen. 2010. "Construction of Fisheye Lens Inverse Perspective Mapping Model and Its Applications of Obstacle Detection." *Hindawi Publishing Corporation EURASIP Journal on Advances in Signal Processing* 2010.

Chuang, W., and S. Zhong-Ke. 2012. "A Novel Traffic Stream Detection Method Based on Inverse Perspective Mapping." *Procedia Engineering* 29: 1938–1943. doi:10.1016/j.proeng.2012.01.240.

Criminisi, A., I. Reid, and A. Zisserman. 1999". "A Plane Measuring Device"." *Image and Vision Computing* 17 (8): 625-634. doi:10.1016/S0262-8856(98)00183-8.

Cucchiara, R., M. Piccardi, and P. Mello. 2000. "Image Analysis and Rule-Based Reasoning for a Traffic Monitoring System." *IEEE Transactions on Intelligent Transportation Systems* 1 (2): 119–130. doi:10.1109/6979.880969.

Daiming, Z., F. Bin, Y. Weibin, L. Xiaosong, and T. Yuanyan. 2014. "Robust Inverse Perspective Mapping Based on Vanishing Point." Proceedings 2014 IEEE International Conference on Security, Pattern Analysis, and Cybernetics (SPAC), Oct, Wuhan, China.

Deng, W., R. Yao, H. Zhao, X. Yang, and L. Guangyu. 2017. "A Novel Intelligent Diagnosis Method Using Optimal LS-SVM with Improved PSO Algorithm Soft Computing." *Soft Computing*. doi:10.1007/s00500-017-2940-9.

Dong, H., X. Wang, C. Zhang, R.. He, L. Jia, and Y. Qin. 2018. "Improved Robust Vehicle Detection and Identification Based on Single Magnetic Sensor." *Ieee Access* 6: 5247-5255. doi:10.1109/ACCESS.2018.2791446. January.

Gang, Y. J., C. Tae Young, H. Suk Kyo, B. Jae Wook, and B. Suk S.. 2000. "Lane and Obstacle Detection Based on Fast Inverse Perspective Mapping Algorithm." IEEE International Conference Systems, Man, Cybernetics. Vol. 4, Oct 2000, Nashville, TN, USA.

Gu, B.., X. Sun, and V. S. Sheng. 2017 JULY. "Structural Minimax Probability Machine." *Ieee Transactions on Neural Networks and Learning Systems* 28 (7): 1646-1656. doi:10.1109/TNNLS.2016.2544779

Hanspeter, A. M., H. H. Bülthoff, J. J. Little, and S. Bohrer. 1991. "Inverse Perspective Mapping Simplifies Optical Flow Computation and Obstacle Detection." *Biological Cybernetics* 64 (3): 177–185. doi:10.1007/BF00201978.

Herbon, C., K. Tönnies, and B. Stock. 2014. *Detection and Segmentation of Clustered Objects by Using Iterative Classification, Segmentation, and Gaussian Mixture Models and Application to Wood Log Detection*, 354–364. Vol. 8753. Switzerland: Springer International Publishing.

Hilleary, T., and T. Omar. 2012. *A Radar Vehicle Detection System for Four-Quadrant Gate Warning Systems and Blocked Crossing Detection*. Washington: Federal Railroad Administration.

Horne, D., D. Findley, D. G. Coble, T. J. Rickabaugh, and J. B. Martin. 2016 September. "Evaluation of Radar Vehicle Detection at Four Quadrant Gate Rail Crossings." *Journal of Rail Transport Planning & Management* 6 (2): 149–162. doi:10.1016/j.jrtpm.2016.04.001.

Hough transform. 2019. [online]. Accessed January 2019. http://www.ic.unicamp.br/~rocha/teaching/2013s1/mc851/aulas/hough-transform.pdf (current)

Hsieh, J.-W., W.-F. Hu, C.-J. Chang, and Y.-S. Chen. 2003. "Shadow Elimination for Effective Moving Object Detection by Gaussian Shadow Modeling." *Image and Vision Computing* 21 (6): 505–516. doi:10.1016/S0262-8856(03)00030-1.

Huang, J.-B., and C.-S. Chen. 2009. "Moving Cast Shadow Detection Using Physics-Based Features." IEEE Conference on Computer Vision and Pattern Recognition, 2310–2317, Miami, FL.

Kamkar, S., and R. Safabakhsh. 2016. "Vehicle Detection, Counting and Classification in Various Conditions." *IET Intelligent Transport Systems* 10 (6): 406–413.

Khairdoost, N., S. A. Monadjemi, and K. Jamshidi. 2013. "Front and Rear Vehicle Detection Using Hypothesis Generation and Verification." *Signal Image Process* 4 (4): 31-50.

Khare, M., R. K. Srivastava, and A. Khare. 2014. "Moving Shadow Detection and Removal a Wavelet Transform Based Approach." *IET Computer Vision* 8 (6): 701–717. doi:10.1049/iet-cvi.2014.0028.

Kim, S., and W. Eun. 1998. "Performance Comparison of Loop/Piezo and Ultrasonic Sensor-Based Traffic Detection System for Collecting Individual Vehicle Information." Processing of The 5th Word Congress on Intelligent Transport Systems, Oct, Seoul, Korea.

Kuo, Y. C., N. S. Pai, and Y. F. Li. 2011. "Vision-Based Vehicle Detection for a Driver Assistance System." *Computers & Mathematics with Applications* 61 (8): 2096–2100. doi:10.1016/j.camwa.2010.08.081.

Leone, A., and C. Distante. 2007. "Shadow Detection for Moving Objects Based on Texture Analysis." *Pattern Recognition* 40 (4): 1222–1233. doi:10.1016/j.patcog.2006.09.017.

Li, Q. L., and J. F. He. 2011. "Vehicles Detection Based on Three Frame Difference Method and Cross-Entropy Threshold Method." *Computer Engineering* 37 (4): 172–174.

Liang, M., X. Huang, C. H. Chen, X. Chen, and A. Tokuta. 2015. "Counting and Classification of Highway Vehicles by Regression Analysis." *IEEE Transaction on Intelligent Transportation Systems* 16: 2878–2888. doi:10.1109/TITS.2015.2424917.

Markevicius, V., D. Navikas, M. Zilys, and D. Andriukaitis. 2016. "Algimantas Valinevicius and Mindaugas Cepenas, "Dynamic Vehicle Detection via the Use of Magnetic Field Sensors"." *Sensors* 16. doi:10.3390/s16122100.

Martel-Brisson, N., and A. Zaccarin. 2008. "Kernel-Based Learning of Cast Shadows from a Physical Model of Light Sources and Surfaces for Low-Level Segmentation." IEEE Conference on Computer Vision and Pattern Recognition, 1–8, Anchorage, AK, USA.

Micheli, F., Alessandro Mecocci, "Real-time Identification Of Vehicles on Highways by 3d Model Matching under Stop-and-go Conditions", 2008, Conference: First Annual International Symposium on Vehicular Computing Systems, Dublin, Irland

Mu, K., F. Hui, X. Zhao, and C. Prehofer. 2016. "Multiscale Edge Fusion for Vehicle Detection Based on Difference of Gaussian." *Optik - International Journal for Light and Electron Optics* 127 (11): 4794–4798. doi:10.1016/j.ijleo.2016.01.017.

Muad, A. M., A. Hussain, S. A. Samad, M. M. Mustaffa, and B. Y. Majlis. 2004. "Implementation of Inverse Perspective Mapping Algorithm for the Development of an Automatic Lane Tracking System." In Proceedings of IEEE Region 10 Conference TENCON, 207–210 November, Chiang Mai, Thailand.

Niknejad, H. T., A. Takeuchi, S. Mita, and D. McAllester. 2012. "On-Road Multivehicle Tracking Using Deformable Object Model and Particle Filter with Improved Likelihood Estimation." *IEEE Transactions on Intelligent Transpotation Systems* 13 (2): 748–758. doi:10.1109/TITS.2012.2187894.

Ohn-Bar, E., and M. M. Trivedi. 2015 March. "Learning to Detect Vehicles by Clustering Appearance Patterns." *IEEE Transactions on Intelligent Transportation Systems* 16: 2511–2521. doi:10.1109/TITS.2015.2409889.

Ramakrishnan, Veena. 2012. "Kethsy a Prabhavathy and J Devishree. Article: a Survey on Vehicle Detection Techniques in Aerial Surveillance." *International Journal Of Computer Applications* 55 (18, October): 43-47.

Sanin, A., Conrad Sanderson, and B. C. Lovell. 2012. "Shadow Detection: A Survey and Comparative Evaluation of Recent Methods." *Pattern Recognition* 45 (4): 1684–1695. doi:10.1016/j.patcog.2011.10.001.

Satzoda, R. K., E. Ohn-Bar, J. Lee, H. Song, and M. M. Trivedi. 2014. "On-Road Vehicle Detection with Monocular Camera for Embedded Realization: Robust Algorithms and Evaluations." International SoC Design Conference (ISOCC), South Korea.

Sheik Mohammed Ali, S., B. George, L. Vanajakshi, and J. Venkatraman. 2011 December. "A Multiple Inductive Loop Vehicle Detection System for Heterogeneous and Lane-Less Traffic." *IEEE Instrumentation and Measurement Society* 61: 1353–1360. doi:10.1109/TIM.2011.2175037.

Shen, X.-L. 2007. "Vision Detection Of Lanes and Vehicles for Advanced Safety Vehicles, Institute Of Computer Science and Information Engineering National Central University Chung-li, Taiwan 320." In *Master Of Computer Science and Information Engineering*, 1-102.

Shoaib, M., R. Dragon, and J. Ostermann. 2009. "Shadow Detection for Moving Humans Using Gradient-Based Background Subtraction." IEEE International Conference on Acoustics, Speech and Signal Processing, 773–776, Taipei, Taiwan.

Sivaraman, S., and M. M. Trivedi. 2013. "Vehicle Detection by Independent Parts for Urban Driver Assistance." *IEEE Transactions on Intelligent Transportation Systems* 14 (4): 1597–1608. doi:10.1109/TITS.2013.2264314.

Stauffer, C., and W. E. L. Grimson. 1999. "Adaptive Background Mixture Models for Real-Time Tracking." Proc IEEE Conf on Comp Vision and Patt Recog (CVPR 1999), 246–252, Ft. Collins, CO.

Sun, B., and S. Li. 2010. "Moving Cast Shadow Detection of Vehicle Using Combined Color Models." Chinese Conference on Pattern Recognition, 1–5, Chongqing, China.

Sun, Z., G. Bebis, and R. Miller. 2005. "On-Road Vehicle Detection Using Evolutionary Gabor Filter Optimization." *IEEE Transactions on Intelligent Transportation Systems* 6 (2): 125–137. doi:10.1109/TITS.2005.848363.

Szwoch, G., and P. Dalka. 2014. *Detection of a Vehicles Stopping in Restricted Zones in Video Suvirance Camera*, 242–253. Switzerland: Springer international publishing.

Tian, B., Y. Li, B. Li, and D. Wen. 2014 April. "Rear-view Vehicle Detection and Tracking by Combining Multiple Parts for Complex Urban Surveillance." *Ieee Transactions on Intelligent Transportation Systems* 15 (2): 597-606.

Tsai, L., J. Hsieh, and K. Fan. 2007. "Vehicle Detection Using Normalized Color and Edge Map." *IEEE Transactions on Image Processing* 16 (3): 850–864.

Tsai, V. J. D. 2006. "A Comparative Study on Shadow Compensation of Color Aerial Images in Invariant Color Models." *IEEE Transaction on Geoscience and Remote Sensing* 44: 1661–1671. doi:10.1109/TGRS.2006.869980.

Umbaugh, Scott E 1998, Computer vision and image processing: a practical approach using CVIPtools, Prentice Hall PTR, Upper Saddle River, NJ

Velazquez-Pupo, R., A. Sierra-Romero, D. Torres-Roman, Y. V. Shkvarko, J. Santiago-Paz, D. Gómez-Gutiérrez, D. Robles-Valdez, F. Hermosillo-Reynoso, and M. Romero-Delgado. 2018. "Vehicle Detection with Occlusion Handling, Tracking, and OC-SVM Classification: A High Performance Vision-Based System." *Sensors* 18 (2): 374. doi:10.3390/s18020374.

Viola, P., and M. Jones. 2001. "Rapid Object Detection Using a Boosted Cascade of Simple Features." In Proc. of the 2001 IEEE Computer Society Conference on Computer Vision and Pattern Recognition, Vol. 1, I–511, Kauai, Hawaii, USA. doi:10.1111/j.1567-1364.2001.tb00001.x.

Wang, B., G. Xiaodu, M. Li, and S. Yan. 2017. "Temperature Error Correction Based on BP Neural Network in Meteorological WSN." *International Journal of Sensor Networks* 23 (4): 265–278. doi:10.1504/IJSNET.2017.083532.

Wang, Y. 2010 Sep. "Joint Random Field Model for All-Weather Moving Vehicle Detection." *IEEE Transaction on Image Process* 19 (9): 2491–2501. doi:10.1109/TIP.2009.2038814.

Wu, B-F.., and J.-H. Juang. 2012. "Adaptive Vehicle Detector Approach for Complex Environments." *Ieee Transactions on Intelligent Transportation Systems* 13 (2) (JUNE): 817-827. doi:10.1109/TITS.2011.2181366.

Yaghoobi Ershadi, N., and J. M. Menéndez 2017 August. "Vehicle Tracking and Counting System in Dusty Weather with Vibrating Camera Conditions." Journal of Sensors: 1-9. doi:10.1155/2017/3812301.24.

Yaghoobi Ershadi, N., J. M. Menéndez, and D.. Jiménez Bermejo. 2017. "Improving Vehicle Tracking Rate and Speed Estimation in Dusty and Snowy Weather Conditions with a Vibrating Camera." *Plos One* 12 (2, December): 1-17.

Yong, S., Y. Fan, and W. Runsheng. 2007. "Color Space Selection for Moving Shadow Elimination." Fourth International Conference on Image and Graphics (ICIG 2007), 496–501, Sichuan, China. doi:10.1094/PDIS-91-4-0467B.

Yuan, C., X. Sun, and L. V. Rui. 2016. "Fingerprint Liveness Detection Based on Multi-Scale LPQ and PCA." *China Communications* 13, (7): 60–65. doi:10.1109/CC.2016.7559076.

Yuhong, J., Y. Xiaoxi, D. Jiangyan, H. Wanjun, K. Jun, and Q. Miao. 2013. "A Novel Moving Cast Shadow Detection of Vehicles in Traffic Scene." *Intelligent Science and Intelligent Data Engineering* 7751: 115–124.

Yunda, S., Y. Baozong, M. Zhenjiang, and W. Wei. 2004. "From GMM to HGMM: An Approach in Moving Object Detection." *Computing and Informatics* 23 (3): 215–237.

Zhang, R., G. Pingshu, X. Zhou, T. Jiang, and R. Wang. 2013. "An Method for Vehicle-Flow Detection and Tracking in Real-Time Based on Gaussian Mixture Distribution." *Advances in Mechanical Engineering* 5. doi:10.1155/2013/861321.

Zhao, Y., and Yi. Su. 2017. "Vehicles Detection in Complex Urban Scenes Using Gaussian Mixture Model with Fmcw Radar." *Ieeeieee Sensors Journal* 17 (18): 5948–5953. doi: 10.1109/JSEN.2017.2733223.

Zhu, H., Y. Fengqi, H. Zhiqiang, L. Chen, and Z. Zhang. 2014. "A Robust Vehicle Detection Algorithm Based on Wireless Sensor Network." 4th IEEE International Conference on Information Science and Technology (ICIST), April, Shenzhen, China.

ZiYang, L., and S. C. Pun-Cheng. 2018 January. "Vehicle Detection in Intelligent Transportation Systems and Its Applications under Varying Environments: A Review." *Image and Vision Computing* 69: 143–154. doi:10.1016/j.imavis.2017.09.008.